Available online at www.sciencedirect.com

ScienceDirect

Underground Space 1 (2016) 62–77

www.elsevier.com/locate/undsp

Investigation of the overconsolidation and structural behavior of Shanghai clays by element testing and constitutive modeling

Guan-lin Ye [a,*], Bin Ye [b]

[a] Department of Civil Engineering and State Key Laboratory of Ocean Engineering, Shanghai Jiao Tong University, Shanghai 200240, China
[b] Department of Geotechnical Engineering, Tongji University, Shanghai 200092, China

Received 11 July 2016; received in revised form 13 August 2016; accepted 18 August 2016
Available online 13 September 2016

Abstract

The mechanical properties and constitutive modeling of Shanghai clays are very important for numerical analysis on geotechnical engineering in Shanghai, where continuous layers of soft clays run 30–40 m deep. The clays are divided into 5 major layers. A series of laboratory tests are carried out to investigate their mechanical properties. The top and bottom layers are overconsolidated hard clays, and the middle layers are normally consolidated or lightly overconsolidated sensitive marine clays. A constitutive model, which can describe the overconsolidation and structure of soils using only 8 parameters, is modified to simulate the test results. A rational procedure to determine the values of the material parameters and initial conditions is also proposed. The model is able to effectively reproduce both one-dimensional (1D) consolidation and drained/undrained triaxial test results of Shanghai clays, with one set of parameters for each layer. From element testing and constitutive modeling, two findings are obtained. First, the decay rates of overconsolidation are smaller in overconsolidated layers than in normally consolidated layers. Second, the natural microstructure of layer 4 is relatively stable, that is, a large degree of structure is still maintained in the specimen even after 1D consolidation and drained triaxial tests. The modified model and obtained parameter values can be used for numerical analysis of geotechnical projects in Shanghai.

Keywords: Shanghai clays; Laboratory tests; Constitutive model; Overconsolidation; Structure

1. Introduction

The mechanical properties of regional soft soils have always attracted the special attention of geotechnical engineers. Shanghai clays are typical soft deltaic deposits with a thickness of 30–40 m. The clays are almost horizontally distributed, representing a fully Holocene transgression-regression sequence in the Yangtze Delta area, China. The clays are divided into 5 major layers, and every layer possesses different physical and mechanical characteristics due to differences in depositional history. These unique characteristics lead to challenges in soil mechanics research. To better understand the mechanical behavior of the different layers and to provide a useful tool for numerical simulations of geotechnical projects in the Shanghai area, systematic laboratory testing and unified constitutive modeling of these layers are of great importance.

In recent decades, much research in the field of geotechnical engineering in Shanghai has been conducted; this includes land subsidence, long-term settlement of subway tunnels, and various underground construction projects (Gao, Wei, & Hu, 1986; Chai, Shen, Zhu, & Zhang, 2004; Chen, Zhang, Zhang, Zhu, & Wang, 2013; Huang, Ye, & Chen, 2009; Liu, Ng, & Wang, 2005; Shen, Wu, Cui, & Yin, 2014; Shen & Xu, 2011; Tan & Wei, 2012;

* Corresponding author.
E-mail addresses: ygl@sjtu.edu.cn (G.-l. Ye), yebin@tongji.edu.cn (B. Ye).

http://dx.doi.org/10.1016/j.undsp.2016.08.001

Wang, Xu, & Wang, 2010). However, studies on the physical and mechanical properties of Shanghai clays are far from being adequate. In general, the limited amount of research on Shanghai clays can be classified into two categories.

(1) The general engineering properties of Shanghai clays without considering the characteristics of the distinct layers (Wei & Hu, 1980; Gao et al., 1986; Xu, Shen, & Du, 2009). Based on site investigations and simple laboratory tests, these studies provided basic data for Shanghai clays, such as the Atterberg limits, cohesive strength (C) and internal friction angle (φ) at different depths. Among these studies, Wei and Hu (1980) investigated the distribution of the overconsolidation ratio (OCR) by laboratory testing and noted that the top and bottom layers of Shanghai clays were overconsolidated, while the layers between the top and bottom could be considered to be normally consolidated to lightly overconsolidated clays (OCR $\approx$ 1.1). Recently, Wu, Ye, Zhang, Bishop, and Wang (2014) noted that besides overconsolidation, the structure was also an important mechanical property of these clays.
(2) Detailed experimental and theoretical study of a specified soil layer. Layer 4, which is the most sensitive and softest stratum in Shanghai clays, has attracted the most research attention. Intensive experiments have been carried out to investigate the effect of fabric/structure on the mechanical behavior of layer 4. De'an, Bo, and Changfu (2014) found that a reference void ratio e^*_{10}, (which is defined as the void ratio on the extended straight line of the compression curve during post-yielding at an effective stress of 10 kPa) could be used as a fabric index to characterize the compression and shear behavior of layer 4. Li, Ng, and Liu (2012) investigated the degree of inherent stiffness anisotropy of layer 3 of Shanghai clays using a triaxial apparatus equipped with local strain transducers and a shear-wave velocity measurement system.

It can be seen that there is a lack of overall detailed experimental and theoretical study on all layers of Shanghai clays. As a result, numerical analyses of underground construction projects in Shanghai had to use empirical methods to determine the material parameters (e.g., Hou, Wang, & Zhang, 2009; Peng, Wang, Tan, Xu, & Li, 2011; Shen, Horpibulsuk, Liao, & Peng, 2009; Shen & Xu, 2011), which is not considered to be a straightforward approach.

Alternatively, in recent years, there has been notable development in creating a constitutive model of overconsolidated and structured clays. For example, Whittle and Kavvadas (1994), Nakai and Hinokio (2004), and Mita, Dasari, and Lo (2004) developed models for overconsolidated clays; Asaoka, Nakano, and Noda. T. (1998), Rouainia and Muir Wood (2000), Liu and Carter (2002), Kimoto and Oka (2005), and Yin, Karstunen, Chang, Koskinen, and Lojander (2011) proposed models for structured clays. Since most of these structural models have a feature that incorporates an inner yielding surface, similar to the bounding surface (Dafalias & Popov, 1975) or subloading surface (Hashiguchi & Ueno, 1977), within a normally yielding surface, they can also describe the overconsolidation of clays.

Zhang, Ye, Noda, Nakano, and Nakai (2007) proposed a constitutive model for sand in which the concepts of superloading (Asaoka, Noda, Yamada, Kaneda, & Nakano, 2002; Asaoka et al., 1998) and subloading (Hashiguchi & Ueno, 1977), together with a new anisotropy approach, were adopted to describe the influences of soil structure, density and stress-induced anisotropy. Compared with previous models, Zhang's model has the following advantages:

(1) The model can describe the static and dynamic behavior of sands under various loading and drainage conditions in a unified way with a fixed set of parameters (Jin, Ye, & Zhang, 2010; Zhang, Ye, & Ye, 2011).
(2) Only 8 material parameters are involved, among which 5 parameters are the same as in the Cam-Clay model, and the other 3 parameters are easily determined.

Therefore, the authors are expecting to extend Zhang's model to simulate the mechanical behavior of Shanghai clays under various loading and drainage conditions in a unified way. The evolution law for the soil structure, however, was only related to the plastic shear strain. This law is not adequate for clays, since plastic volumetric strain can also lead to the loss of structure.

In this study, a brief introduction of Shanghai clays and laboratory test results are presented. A modified version of Zhang's model with new evolution laws is then proposed. The results of oedometer tests and drained triaxial tests are used to verify the performance of the model. Most importantly, based on the experimental and modeling studies, the overconsolidation and structure characteristics of Shanghai clays are discussed in detail.

2. Brief description of Shanghai clays

Shanghai is located on the extensive Yangtze River Delta. The thickness of Shanghai clays is approximately 30–40 m, with an annual groundwater table that is approximately 1.0 m from the surface. The strata are almost horizontally distributed. The soil layers are defined by a number from the surface to the bottom and named according to their colors and grain size distributions, as shown in the left of Fig. 1. Layer 1 is a thin fill soil, which is omitted in the figure. Layers 2–6 are mainly clays and are widespread in Shanghai. In general, the term 'Shanghai clays' refers to layers 2–6. They consist of the Holocene series (layers 2–5) and the top of the Pleistocene series (layer 6).

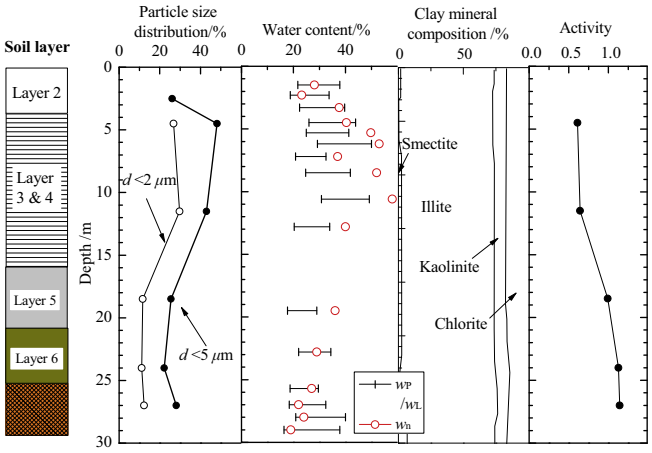

Fig. 1. Typical distributions of physical properties of layer 2–6 of Shanghai clays with depth.

By comparing with the other Asian clays deposited in the same period (Wu et al., 2014), it was found that Shanghai clays exhibit some unique characteristics: (1) Clay particles (<5 μm) and silt particles (75–5 μm) are their main components, accounting for over 50% of the grain size distribution. Meanwhile, clay particles are the main component in other Asian clays. (2) Illite is the most common clay mineral, averaging over 50 %, while smectite is the most common mineral in other Asian clays. (3) The natural water content (w_n) of Shanghai clay is 25–45 %. The w_n of layers 3 and 4 are larger than the liquid limit (w_L), indicating that they are sensitive clays. The activity, defined as the ratio of the plasticity index (I_p) to the clay fraction percentage, varies from 1.0 at the bottom to 0.5 at the top. The activities of other Asian clays are much higher. Fig. 2 shows the plasticity chart of Shanghai clays. It can be seen that they are low plasticity clays. It is worth investigating such unique clays carefully, by element testing and constitutive modeling.

3. Laboratory tests

The undisturbed samples of layers 2–6 were recovered using a Shelby thin-walled tube sampler from a construction site located at Lianhua Road in the Minhang District of Shanghai. The sampling depths at each layer are shown in Fig. 3 with solid circles. In addition, undisturbed samples from layer 4 were used for the drained/undrained triaxial tests, and these were taken by the block sampling method (ASTM D705, 2004) from open excavation sites at Xizha Road/Longhua Tower.

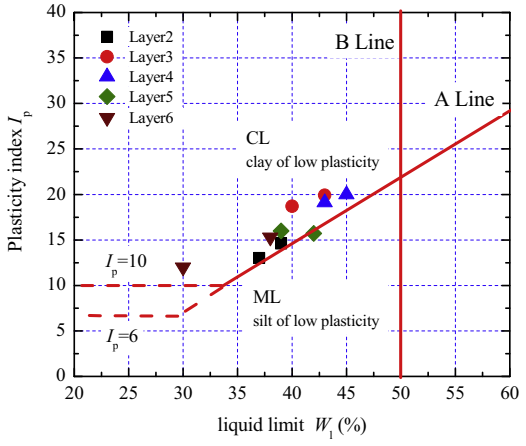

Fig. 2. Plasticity chart of Shanghai clays (layer 2–6).

Conventional oedometer tests and drained triaxial compression tests (CD tests) were carried out on layers 2–6 to investigate the compression and stress–strain relationships of Shanghai clays. In addition, undrained triaxial tests (CU tests) were carried out on layer 4 with the samples from the Longhua Tower site. In the conventional oedometer tests, the specimens were 61.8 mm in diameter and 20 mm in height. Each applied load increment was twice as large as the previous one, and the duration of each load was 24 h. In the triaxial tests, the specimens were 39.1 mm in diameter and 80 mm in height. The triaxial tests consisted of isotropic compression, starting from the stress state when the pore pressure had stabilized and the saturation of the specimens had been confirmed. The shearing rates for drained and undrained triaxial tests were 0.0033 mm/min and 0.0066 mm/min, respectively.

Fig. 3 shows typical distributions of OCR and sensitivity with the depth of Shanghai clays. The OCR data were obtained from conventional oedometer tests, and the sensitivity data were obtained by uniaxial compression tests on undisturbed and remolded samples. It can be seen that layers 2 and 6 are overconsolidated clays, layers 3 and 4 are sensitive clays with a strong structure, and layer 5 is a transition stratum with a slight overconsolidation and low sensitivity. It is interesting to find that as an illite-rich clay, Shanghai clays show a relatively low sensitivity. The overconsolidation of layers 2 and 6 is mainly due to the continental deposition environment and evaporation during the deposition period. The structures of layers 3 and 4 are due to the marine deposition environment. Therefore, it is required that the constitutive model can simulate both

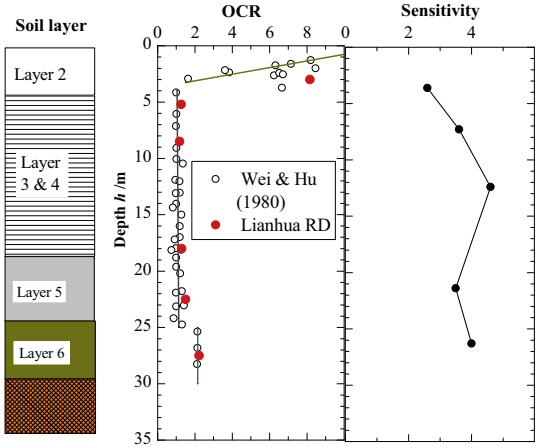

Fig. 3. Typical distributions of OCR (overconsolidation ratio) and sensitivity with depth of layer 2–6 of Shanghai clays. OCR data obtained from conventional oedometer tests. Sensitivity data obtained by uniaxial compression tests.

the overconsolidation and structure of natural clays. More results of the oedometer tests and triaxial tests will be described in Section 7.

4. Constitutive model

Zhang et al. (2007) proposed a constitutive model in which a new approach to the description of anisotropy changes was adopted. The new approach allows the anisotropy of sand to change continuously and rapidly during liquefaction. The model is able to uniquely describe the overall mechanical behavior of sand at different densities, including its dynamic and static behavior under various loading conditions. The authors are expecting to extent Zhang's model to simulate the mechanical behavior of Shanghai clays under various loadings and drainage conditions in a unified way. In the current study, as the first step of the extension, Zhang's model is modified so that it can be used to describe the mechanical behavior of Shanghai clays under static loading.

4.1. Original model

The original model was proposed within the framework of critical state soil mechanics and was based on the concepts of anisotropy (Sekiguchi H, 1977), subloading (Hashiguchi & Ueno, 1977) and superloading (Asaoka et al., 1998, 2002). A brief description of the yield surfaces is presented in Fig. 4.

The similarity ratio of the superloading surface to the normal yield surface, R^*, and the similarity ratio of the superloading surface to the subloading surface, R, are given as:

$$R^* = \frac{\widehat{p}}{\bar{p}} = \frac{\widehat{q}}{\bar{q}},\ 0 < R^* \leqslant 1,\ \text{and}\ \frac{\widehat{q}}{\widehat{p}} = \frac{\bar{q}}{\bar{p}} \tag{1}$$

$$R = \frac{p}{\bar{p}} = \frac{q}{\bar{q}},\ 0 < R \leqslant 1,\ \text{and}\ \frac{\widehat{q}}{\bar{p}} = \frac{\widehat{q}}{\widehat{p}} = \frac{q}{p} \tag{2}$$

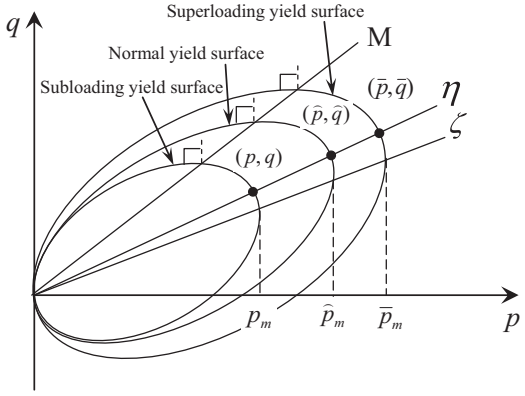

Fig. 4. Subloading, normal and superloading yield surfaces in p–q plane.

where (p, q), $\widehat{p}$, $\widehat{q}$) *and*$(\bar{p}, \bar{q})$ represent the present stress state, the corresponding normally consolidated stress state, and the structured stress state on the p–q plane, respectively. The present stress state is always located on the subloading surface, which is given in the following form:

$$f = \ln\frac{\sigma_m}{\sigma_{m0}} + \ln\frac{M^2 - \zeta^2 + \eta^{*2}}{M^2 - \zeta^2} + \ln R^* - \ln R - \frac{\varepsilon_v^p}{C_p} = 0 \tag{3}$$

In Eq. (3), $\sigma_m = \frac{1}{3}\sigma_{ii}$ is the mean effective stress and $\sigma_{m0} = 98.0$ kPa is a reference stress. M is the shear ratio at the critical state. ε_v^p is the plastic volumetric strain. $\zeta = \sqrt{\frac{3}{2}\beta_{ij}\beta_{ij}}$ is an anisotropic state variable, with β_{ij} as the anisotropic stress tensor. $\eta^* = \sqrt{\frac{3}{2}\hat{\eta}_{ij}\hat{\eta}_{ij}}$ represents the difference between the stress ratio tensor ηij and the anisotropic stress tensor β_{ij}, in which

$$\hat{\eta}_{ij} = \eta_{ij} - \beta_{ij}, \eta_{ij} = \frac{S_{ij}}{\sigma_m}, S_{ij} = \sigma_{ij} - p\delta_{ij}, \tag{4}$$

where S_{ij} is the deviatoric stress tensor and δ_{ij} is the Kronecker delta tensor. $\hat{\eta}_{ij}$ is a relative shear stress ratio tensor. In Eq. (3), C_p is expressed as:

$$C_p = \frac{\lambda - k}{1 + e_0} \tag{5}$$

where λ and κ are the compression and swelling indices, respectively, and e_0 is a reference void ratio at pressure $p = 98$ kPa.

An associated flow rule is employed in the model:

$$d\varepsilon_{ij}^p = \Lambda\frac{\partial f}{\partial \sigma_{ij}} \tag{6}$$

The consistency equation for the subloading yield surface can then be given as:

$$\begin{aligned} df &= 0 \\ &\Rightarrow \frac{\partial f}{\partial \sigma_{ij}}d\sigma_{ij} + \frac{\partial f}{\partial \beta_{ij}}d\beta_{ij} + \frac{1}{R^*}dR^* - \frac{1}{R}dR - \frac{1}{C_p}d\varepsilon_v^p \\ &= 0 \end{aligned} \tag{7}$$

The evolution rule for the degree of structure, R^*, is defined as:

$$dR^* = U^* d\varepsilon_d^p,\ U^* = \frac{a\mathrm{M}}{C_p}R^*(1 - R^*) \quad (0 < R^* \leqslant 1), \tag{8}$$

where a is a parameter that controls the rate of structure collapse during shearing and $d\varepsilon_d^p$ is the deviatoric plastic strain.

The changing rate of overconsolidation is assumed to be controlled by two factors: the plastic component of strain and the incremental anisotropy:

$$dR = U\|d\varepsilon_{ij}^p\| + R\frac{\eta}{M}\frac{\partial f}{\partial \beta_{ij}}d\beta_{ij}, \tag{9}$$

where

$$\|d\varepsilon_{ij}^{p}\| = \sqrt{d\varepsilon_{ij}^{p} d\varepsilon_{ij}^{p}} = \Lambda \sqrt{\frac{\partial f}{\partial \sigma_{ij}} \frac{\partial f}{\partial \sigma_{ij}}} = \Lambda \frac{\sqrt{6\eta^{*2} + \frac{1}{3}(M^2 - \eta^2)^2}}{(M^2 - \zeta^2 + \eta^{*2})\sigma_m} \tag{10}$$

$$U = -\frac{m\mathrm{M}}{C_\mathrm{p}} \left(\frac{(\sigma_m/\sigma_{m0})^2}{(\sigma_m/\sigma_{m0})^2 + 1} \right) \ln R \quad (\sigma_{m0}: \text{ reference stress, } = 98.0 \text{ kPa}) \tag{11}$$

Here, m is a parameter that controls the losing rate for overconsolidation.

The evolution rule for the anisotropic stress tensor is defined as:

$$d\beta_{ij} = \frac{M}{C_\mathrm{p}} b_\mathrm{r}(M - \zeta) d\varepsilon_d^p \frac{\hat{\eta}_{ij}}{\|\hat{\eta}_{ij}\|} = \sqrt{\frac{3}{2}} \frac{M}{C_\mathrm{p}} b_\mathrm{r}(M - \zeta) d\varepsilon_d^p \frac{\hat{\eta}_{ij}}{\eta^*}, \tag{12}$$

where b_r is a parameter that controls the developing rate of anisotropy.

If the incremental strain tensor is divided into elastic and plastic components, the elastic component is as follows:

$$d\sigma_{ij} = E_{ijkl} d\varepsilon_{kl}^{e} = E_{ijkl}(d\varepsilon_{kl} - d\varepsilon_{kl}^{p}) = E_{ijkl} d\varepsilon_{kl} - \Lambda E_{ijkl} \frac{\partial f}{\partial \sigma_{kl}} \tag{13}$$

Therefore, by substituting Eqs. (8), (9), (12) and (13) into Eq. (7), the positive variable can be rewritten as:

$$\Lambda = \frac{\frac{\partial f}{\partial \sigma_{ij}} E_{ijkl} d\varepsilon_{kl}}{h_p + \frac{\partial f}{\partial \sigma_{ij}} E_{ijkl} \frac{\partial f}{\partial \sigma_{kl}}}, \tag{14}$$

where:

$$h_\mathrm{p} = \frac{1}{C_\mathrm{p}(M^2 - \zeta^2 + \eta^{*2})\sigma_m} [M_s^2 - \eta^2] \tag{15}$$

$$M_\mathrm{s}^2 = M^2 - \frac{mM \ln R}{R} \left[\frac{(\sigma_m/\sigma_{m0})^2}{(\sigma_m/\sigma_{m0})^2 + 1} \right] \sqrt{6\eta^{*2} + \frac{1}{3}(M^2 - \eta^2)^2} - 2aM(1 - R^*)\eta^* + \left(1 - \frac{\eta}{M}\right) \frac{\sqrt{6} M b_\mathrm{r}(M - \zeta)\eta^{*2}(2M^2 - 3\eta_{ij}\beta_{ij})}{(M^2 - \zeta^2 + \eta^{*2})(M^2 - \zeta^2)} \tag{16}$$

The loading criteria are as follows:

$$\begin{cases} \Lambda > 0 & \text{loading} \\ \Lambda = 0 & \text{neutral} \\ \Lambda < 0 & \text{unloading} \end{cases} \tag{17}$$

Eight parameters are involved in the proposed model, among which five parameters, i.e., M, e_0, λ, κ and ν, are the same as in the Cam-Clay model. The other three parameters are listed below:

m: parameter that controls the decaying rate of overconsolidation.
a: parameter that controls the collapse rate of structure.
b_r: parameter that controls the developing rate of stress-induced anisotropy.

These three parameters have clear physical meanings and can be readily determined through laboratory testing.

The capability of the model in simulating Toyoura sand, which is a typical clean sand found in Japan, is demonstrated in the Appendix. The model has also been successfully applied to numerical analyses of various liquefaction phenomena (Bao, Ye, Ye, & Zhang, 2012; Bao, Ye, Ye, Sago, & Zhang, 2014; Xia, Ye, Wang, Ye, & Zhang, 2010; Ye, Muramatsu, Ye, & Zhang, 2011; Ye, Ye, & Zhang, 2012; Ye, Ye, Zhang, & Yashima, 2007; Zhang et al., 2011). Therefore, it is a promising model with great potential for simulating the mechanical behavior of Shanghai clays under various loadings and drainage conditions in a unified way.

4.2. New evolution law

In the original model, the evolution rule for the degree of structure, R^*, is a function of the plastic shear strain $d\varepsilon_d^p$. However, some experimental studies on natural clays (e.g., Callisto & Rampello, 2004) have proved that both the plastic volumetric strain and plastic shear strain can lead to the loss of structure. In the current study, the degradation of structure is assumed to be a function of $\|d\varepsilon_{ij}^p\|$, and a new evolution law for structure is proposed as follows:

$$dR^* = U^* \|d\varepsilon_{ij}^p\|, \tag{8a}$$

The definition of U^* is the same as in Eq. (8).

Furthermore, in the original model, to describe the cyclic mobility behavior of liquefied sand, $\left(\frac{(\sigma_m/\sigma_{m0})^2}{(\sigma_m/\sigma_{m0})^2+1}\right)$ was added into the first term in Eq. (10). The reference stress, σ_{m0}, is normally set to 98.0 kPa. This can keep the U as small as possible when σ_m is close to zero (liquefaction point), so that the large overconsolidation can help the effective stress path diverge from the liquefaction point. However, it is unlikely that the overconsolidation of clays can increase when σ_m is small. It was found that an unnatural compression would occur when $\sigma_m < \sigma_{m0}$ (=98.0 kPa) in the simulation of 1D consolidation of clays using the original model. To avoid this unnatural compression, σ_{m0} is set to 1.0 kPa for clayey soils.

Consequently, the positive variable Λ remains the same as in Eq. (14), and M_s^2 in Eq. (15) is rewritten as follows:

$$M_\mathrm{s}^2 = M^2 - \left(aM(1 - R^*) + \frac{mM \ln R}{R} \frac{(\sigma_m/\sigma_{m0})^2}{(\sigma_m/\sigma_{m0})^2 + 1} \right) \times \sqrt{6\eta^{*2} + \frac{1}{3}(M^2 - \eta^2)^2} + \frac{4Mb_\mathrm{r}\eta^{*2}\left(\eta^* - \sqrt{3/2}\hat{\eta}_{ij}\beta_{ij}\right)}{(M^2 + \eta^{*2})} \tag{16a}$$

5. Material parameters, initial conditions and simulation procedure

To simulate the results of oedometer tests and drained triaxial tests for each soil layer with one set of material parameters using the modified constitutive model, the

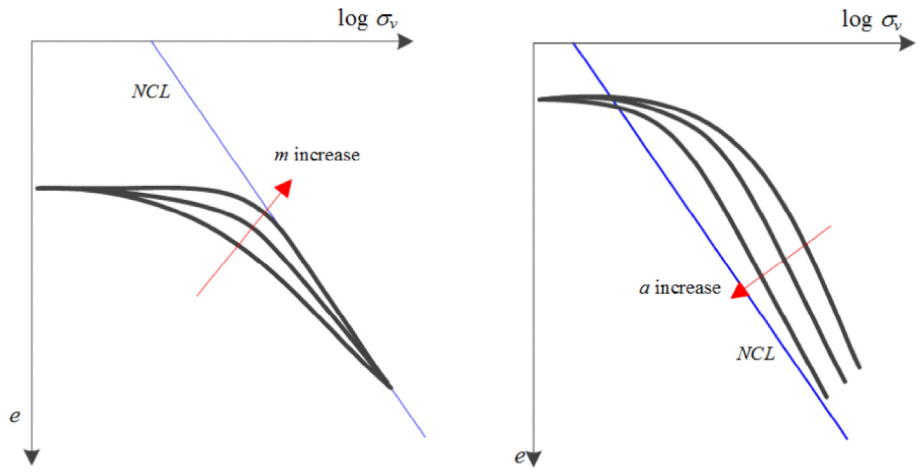

(a) Overconsolidated clay (b) Structured clay

Fig. 5. Influence of parameters m and a to the shape of e-logσ_v curve. (a): as m increases, shifting rate from overconsolidation to normally consolidated state increases. (b): as a increases, losing rate of structure increases.

Table 1
Material parameters used for comparison with Modified Cam-clay model.

Parameters	Values
Compression index λ	0.1
Swelling index κ	0.02
Critical state parameter M	1.20
Void ratio e_0 (p = 98 kPa on $N.C.L.$)	1.0
Poisson's ratio v	0.35
Degradation parameter of overconsolidation m	1.0
Degradation parameter of structure a	1.0
Evolution parameter of anisotropy b_r	0.0

Note: The parameters, λ, κ, M, e_0, and v used in MCC model have the same value as above.

Table 2
Initial conditions used for comparison with Modified Cam-clay model.

Initial conditions	Values
Pre-consolidation stress p'_c (kPa)	500
Initial degree of structure R_0^*	0.1
Initial anisotropy ζ_0	0.0

material parameters and initial conditions must be determined in a rational way. Eight parameters and three initial values are involved in the proposed model. Five parameters, i.e., M, e_0, λ, κ and v, are the same as in the Cam-Clay model. They can be determined directly by oedometer tests and triaxial tests. Stress-induced anisotropy is less important in oedometer tests and in isotropically consolidated triaxial tests. Thus, the parameter for controlling stress-induced anisotropy, $b_{r,}$ and the initial value of anisotropy, ζ_0, are taken as zero in the current study. The other two evolution parameters for overconsolidation and structure, that is, m and a, and the initial values of overconsolidation R_0 and structure R^*_0 of each test can be obtained by the following procedure:

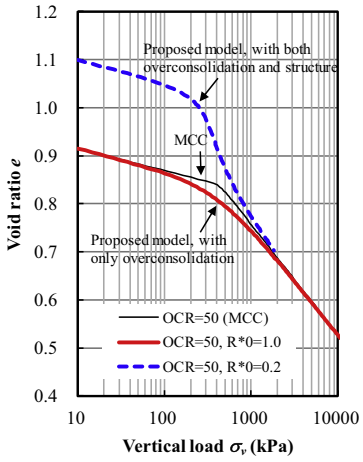

Fig. 6. Comparison of the performance of the new model with Modified Cam-Clay model by simulating clays with overconsolidation and structure in the oedometer tests.

(1) Determining the initial values of overconsolidation R_0 and structure R^*_0.

$R_0 = 1/\text{OCR} =$ pre-consolidation stress/initial confining stress. From experience, due to the rounded shape of e-logσ_v curves of Shanghai clays, the pre-consolidation stress can be obtained more easily by the 'work criterion' method of Becker, Crooks, Been, and Jefferies (1987) than by Casagrande's graphical method. σ_v is the effective vertical stress.

$R^*_0 = 1/\text{Sensitivity}$. The sensitivity is the ratio of the undrained strength of the undisturbed clay to the reconstituted strength at the same moisture content. In the current study, its value is determined by the uniaxial compression tests. However, it is recognized that the value of sensitivity may vary according to the investigation methods used. Thus, in the simulation, the value may need to be adjusted to fit the test results.

(2) Determining the values of m and a by fitting the oedometer tests.

The initial values of overconsolidation R_0 and structure R^*_0 and the reference void ratio e_0 determine the starting point and turning point of the void ratio – effective vertical stress (e-$log\sigma_v$) curve and parameters m and a determine the shape of the e-$log\sigma_v$ curve. The influence of m and a on the shape of the e-$log\sigma_v$ curve is shown in Fig. 5. The definitions of m and a are given in Eq. (11) and (8), respectively. m is the parameter controlling the shift speed from overconsolidation to the normally consolidated state. The larger the value of m, the larger the curvature of the e-$log\sigma_v$ curve. a is the parameter controlling the loss rate of structure. The larger the value of a, the faster the e-$log\sigma_v$ curve will revert back to the normal-consolidation line (NCL).

By making use of the evolution laws for overconsolidation and structure, the initial conditions for triaxial tests with different confining stresses can be traced easily. With the material parameters and initial conditions that fitted the e-$log\sigma_v$ curves of the oedometer tests, a simulation of the isotropic consolidation is conducted to obtain the initial state (values of R and R^*) for each triaxial compression test. The simulation starts at a confining stress of 10 kPa, and the values of R and R^* at each prescribed confining stress value are taken as the initial state for the corresponding triaxial compression test. Then, simulations of triaxial compression tests are carried out.

6. Comparison with Modified Cam-Clay model

Quantitative comparisons between the performances of the modified model and Modified Cam-Clay (MCC) model are shown in Figs. 6–8. The parameters and initial conditions used for these simulations are listed in Tables 1 and 2. Two types of tests are considered in the simulation. The first is the one-dimensional oedometer tests, which started with a vertical load of 10 kPa. The second type is the conventional isotropic consolidated – drained triaxial compression tests with constant confining pressures of 100 kPa.

Figs. 6 and 7 show the simulations that only consider overconsolidation. It can be seen that compared to the MCC model, the modified model can represent the rounded $e \sim log\sigma_v$ curve of the oedometer tests and the rounded stress–strain-dilatancy curves crossing over the peak strengths in the triaxial tests. These indicate that the modified model can give a smooth transition from the overconsolidated state to the normally consolidated state, generally resulting in a better match to real life situation (Muir Wood, Belkheir, & Liu, 1994).

The dashed lines in Fig. 8 show the simulation that only considers structure (OCR = 1, $R^*_0 = 0.2$). It appears that the modified model can describe the typical behavior of normally consolidated clays with a high degree of structure, that is, a large volumetric compression accompanied by strain-hardening during shearing. This behavior cannot be described by the MCC model. Simulations considering both overconsolidation and structure are also given in Figs. 6 and 8 respectively. In the oedometer tests, the void ratio collapses in the $e \sim log\sigma_v$ curve, and in the triaxial tests, the strain-softening and dilatancy due to overconsol-

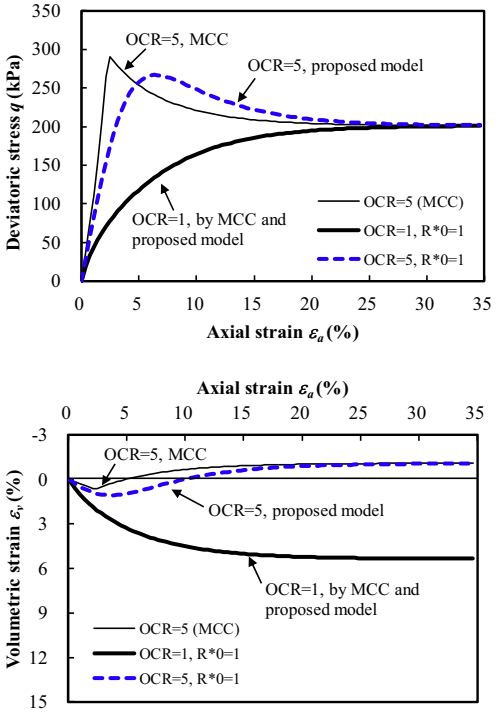

Fig. 7. Comparison of the performance of the new model with Modified Cam-Clay model by simulating the remolded clays with overconsolidation in triaxial tests.

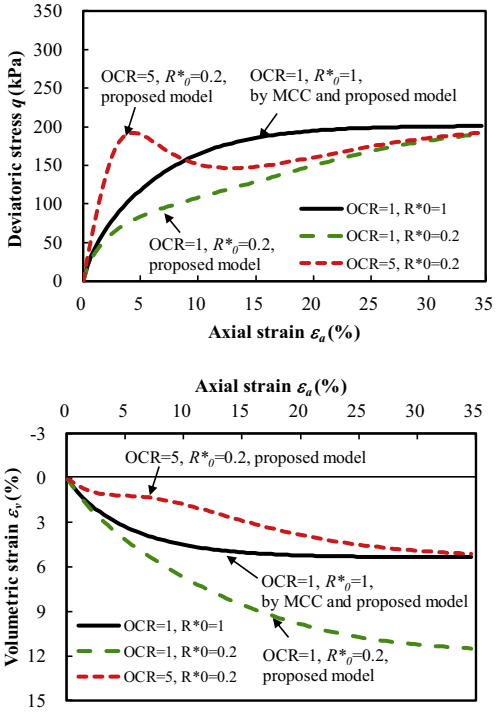

Fig. 8. Comparison of the performance of the new model with Modified Cam-Clay model by simulating the clays with both overconsolidation and structure in triaxial tests.

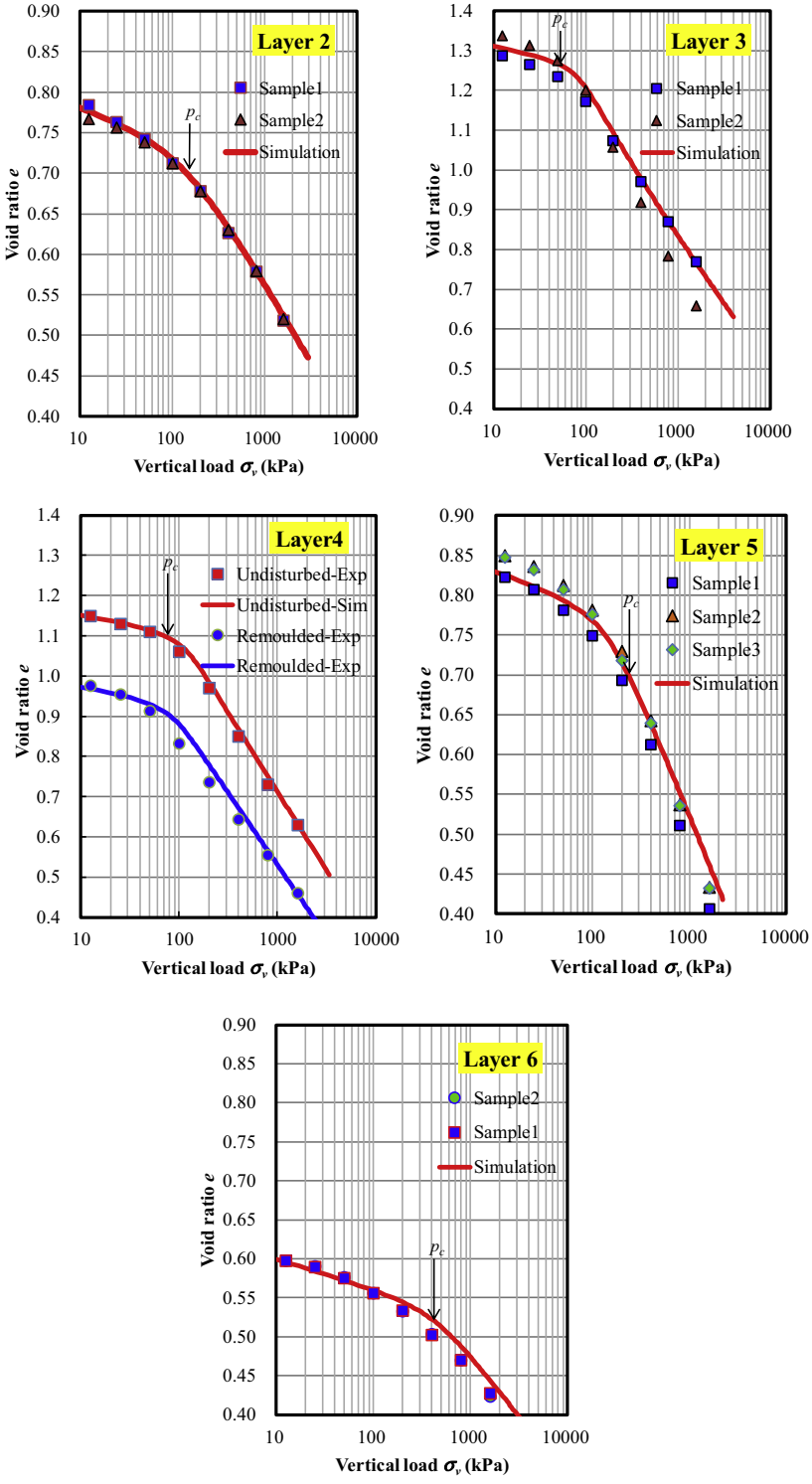

Fig. 9. Test results of oedometer tests on layer 2–6 of Shanghai clays and the Simulation by the modified model.

idation occur before the axial strain $\varepsilon_a < 5$–8%; above this strain, strain-hardening and volumetric compression due to de-structuration takes place.

From the previous descriptions, it can be stated that the modified model cannot only describe the smooth transition from the overconsolidated state to normally consolidated clays but can also describe the de-structuration of soil structure that cannot be presented by the MCC model.

7. Test and simulation results of Shanghai clays

7.1. General mechanical behaviors of Shanghai clays

Fig. 9 shows the test results of one-dimensional oedometer tests for layers 2–6 and the model simulations. Fig. 10 shows the tests results of drained triaxial compression tests (CD tests) for layers 2–6 and the model simulations. Fig. 11

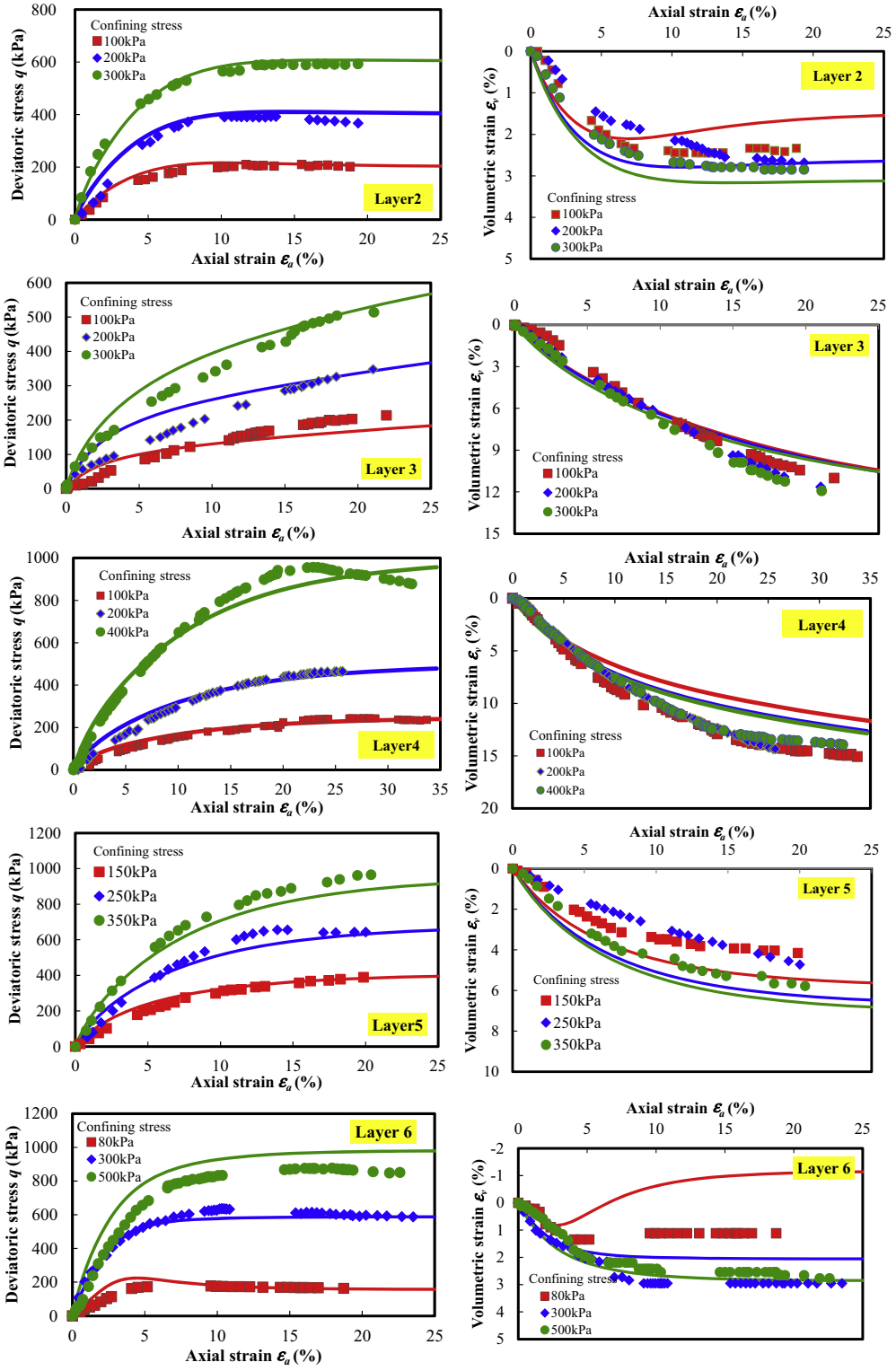

Fig. 10. Test results of CD tests on layer 2–6 of Shanghai clays and the Simulation by the modified model.

shows the tests results of undrained triaxial compression tests (CU tests) for layer 4 and the model simulations. In these figures, the experimental results and model simulations are represented by scatter points and solid lines, respectively. The parameters and initial conditions used for these simulations are listed in Tables 3 and 4. Several conclusions are reached, as follows:

(1) From the *e-log*σ_v curves in Fig. 9, it can be seen that layers 3 and 4 are soft clays characterized by the highest compressibility, while layers 2 and 6 are relatively hard clays with the lowest compressibility. Layer 5 has an intermediate compressibility. This is consistent with the variation of OCR and sensitivity shown in Fig. 4.

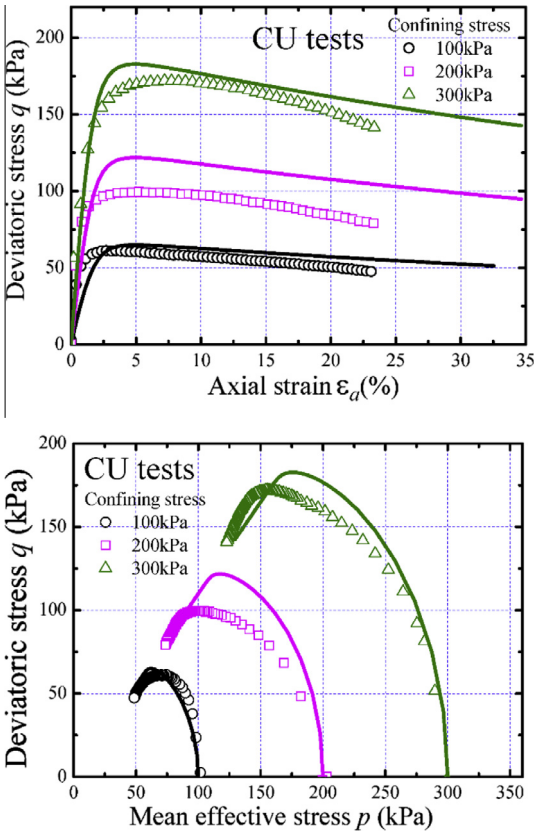

Fig. 11. Test results of CU tests on layer 4 (Longhua Tower) and the Simulation by the modified model.

(2) It can be seen that the curvatures of e-$log\sigma_v$ curves of the overconsolidated layers 2 and 6 are smaller than those of the structured layers 3 and 4, and an obvious non-linear deformation had already occurred before the vertical load reached the pre-consolidation pressure, p_c. This phenomenon cannot be simulated by the Cam-Clay model, which only permits non-linear deformation when a load is greater than p_c.

(3) Fig. 10 shows the stress–strain-dilatancy of the CD tests. The approximate axial strain where the deviatoric stress reaches the peak value for each layer is as follows: 5% to 10% for layers 2 and 6, 15% for layer 5, and >20% for layers 3 and 4. The approximate final compressive volumetric strain of each layer is as follows: 3% for layers 2 and 6, 6% for layer 5, and >12% for layers 3 and 4.

(4) Fig. 11 shows the stress–strain relationship and stress paths of the undrained triaxial compression tests of layer 4. The overall undrained behavior, especially strain-softening due to the collapse of the soil structure, can be well reproduced by the model.

(5) The general trend of overconsolidated clays (layers 2 and 6) can be captured by the new model in terms of the e-$log\sigma_v$ curve and stress–strain-dilatancy relation. The smooth change from an overconsolidated to a normally consolidated state shown in the e-$log\sigma_v$ curve is represented well. The deviatoric stresses and volumetric strains in the triaxial tests are accurately described. However, the dilatancy of layer 6 under low confining stress is overestimated by the model.

The soil structure of layers 2 and 6 is not taken into consideration in the simulation by setting $R_0^* = 1.0$, although both layers have a sensitivity of 2–3. This indicates that the microstructure of this type of overconsolidated clay is not easy to disrupt, and the change in the void ratio is mainly due to the elimination of overconsolidation.

(6) As shown in Fig. 5, parameter m controls the curvature of the e-$log\sigma_v$ curve. Table 3 shows that the m values of layers 2 and 6 (overconsolidated) are much smaller than those of layers 3 and 4 (normally consolidated). Since m is a material parameter, its value should be determined by the material itself, rather than by the initial overconsolidated state. Therefore, from the plasticity chart (Fig. 2), it seems that the m value is likely to increase when the location in the plasticity chart of the corresponding soil moves to the right along the A line.

Table 3
Material parameters of Shanghai clays.

Parameters	Layer 2	Layer 3	Layer 4	Layer 5	Layer 6
Compression index λ	0.087	0.132	0.140	0.135	0.070
Swelling index κ	0.020	0.020	0.020	0.019	0.017
Critical state parameter M	1.20	1.30	1.30	1.42	1.18
Void ratio e_0 (p = 98 kPa on $N.C.L.$)	0.757	1.080	0.860	0.815	0.630
Poisson's ratio v	0.32	0.38	0.38	0.35	0.32
Degradation parameter of overconsolidation m	0.7	4.0	5.0	1.5	1.5
Degradation parameter of structure a	1.0	0.4	0.1	2.0	1.0
Evolution parameter of anisotropy b_r	0.0	0.0	0.0	0.0	0.0

Table 4
Initial conditions of Shanghai clays.

Initial conditions	Layer 2	Layer 3	Layer 4	Layer 5	Layer 6
Pre-consolidation stress p_c' (kPa)	150	65	80	220	410
Initial degree of structure R_0^*	1.0	0.3	0.2	0.6	1.0
Initial anisotropy ζ_0	0.0	0.0	0.0	0.0	0.0

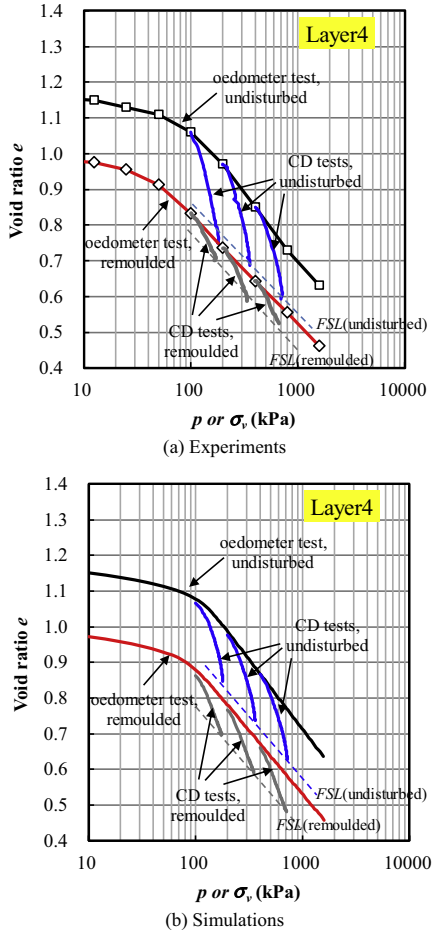

Fig. 12. Plot of oedometer tests and drained triaxial tests of layer 4 in terms of *e-logp* relation.

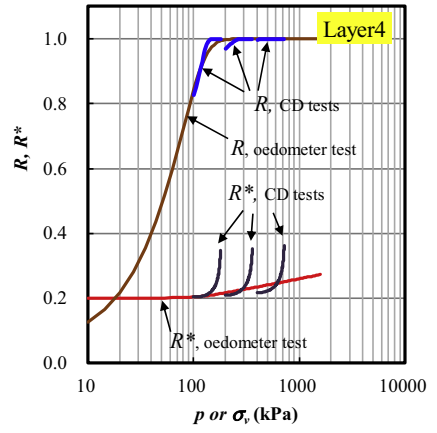

Fig. 13. Changes of R (=1/OCR) and R^* (degree of structure) in the simulations of element tests for undisturbed Layer 4.

(7) The overall behavior of the structured clays (layers 3 and 4) can also be reproduced by the new model. The large volume changes in both the oedometer tests and triaxial tests due to de-structuration are accurately simulated.
(8) Layer 5 is a clay with light overconsolidation and weak structure. Its behavior also can be represented by the model.

7.2. Discussion on the structure of layer 4

As layer 4 is a typical stratum of Shanghai clays, which have the strongest structure, its structure will be discussed further. Fig. 12(a) shows the plot of the oedometer tests and drained triaxial tests of layer 4 in terms of the *e-logp* (for triaxial tests) or *e-log*σ_v (for oedometer tests) relation. The solid curves with symbols and the solid curves represent the oedometer tests and drained triaxial tests, respectively. Fig. 12(b) shows the plot of the simulation results. In both figures, the horizontal axis represents the vertical stress (σ_v) for the oedometer tests and the mean stress for the triaxial tests.

From Fig. 12(a), two findings can be obtained: (1) At the end of the oedometer test, when the final vertical stress is 1600 kPa, the void ratio of the undisturbed specimen is much larger than that of the remolded one. (2) The final state lines (FSL) of the triaxial tests on the undisturbed and remolded specimens are almost parallel, and no trend toward convergence can be seen. The simulations in Fig. 12(b) show the same results. These phenomena reveal that neither the oedometer tests nor triaxial shearing can easily destroy the soil structure. The change in R (=1/OCR) and R^* (degree of structure) in different tests is shown in Fig. 13. The overconsolidation is eliminated very quickly in both the oedometer tests and triaxial tests. In contrast, the structure decays slowly. The initial degree of the structure is $R_0^* = 0.2$, and the final degrees of the structure are $R^* = 0.286$ (in the oedometer tests) and $R^* = 0.35$–0.36 (in the triaxial tests). Although triaxial shearing is more effective in destroying the soil structure, a large portion of the structure still remains despite the specimen being subjected to an axial strain of 35%, which provides evidence that the natural microstructure of layer 4 is relatively stable.

8. Conclusions

In this study, element tests and constitutive modeling were conducted to investigate the overconsolidation and structure of all layers of Shanghai clays. The mechanical characteristics of Shanghai clays became clear through a discussion of both the laboratory test data and the simulation results. The following conclusions can be drawn from the study:

(1) The element tests showed that the top and bottom layers 2 and 6 were overconsolidated clays, the middle layers 3 and 4 were sensitive clays with a strong structure, and layer 5 was a transition stratum with slight overconsolidation and low sensitivity. It was interesting to find that as an illite-rich clay, Shanghai clays showed a relative low sensitivity.
(2) The modified Zhang's constitutive model can describe the overconsolidation and structure of layers 2–6 of Shanghai clays in a unified way. Eight parameters were used, among which five parameters, that is, M, N, λ, κ, and v, were the same as those of the Cam-Clay model. The other three parameters, a, m and b_r,

can be easily determined by the rational procedure proposed in this study.

(3) It was found by constitutive modeling that the decaying rate of overconsolidation is smaller in the overconsolidated layers 2 and 6 than in the normally consolidated layers 3 and 4.

(4) Constitutive modeling of the structural characteristics of layer 4 indicated that a large portion of the structure still remained despite the specimen being subjected to an axial strain of 35%, which provided evidence that the natural microstructure of layer 4 was relatively stable.

In this study, the mechanical behavior of Shanghai clays was analyzed within the framework of the critical state soil mechanics, so that it might assist international colleagues to understand the mechanical characteristics of Shanghai clays. In addition, inherent anisotropy is another important factor on the mechanical behavior of natural clays, and further experimental and numerical studies should be carried out in this area in the future.

Acknowledgements

The first author expresses his appreciation to former student Mr. Jia-ren Sheng, who carried out the laboratory tests. The financial support of the National Nature Science Foundation of China (Grant No. 41372284) is gratefully acknowledged.

Appendix A

Brief description of the capability of Zhang's model on simulating Toyoura sand uniquely

The mechanical behaviors of sand are dependent not only on the shape of particles, that is, angular or round, but also on its density, its experienced strain history, and even on the degree of structure formed in its deposition (Asaoka et al., 1998). Sand may behave completely differently under different loadings and drained conditions. For instance, when subjected to undrained cyclic loading, loose sand will liquefy without transitioning from contractive to dilative state; for medium dense sand, liquefaction with cyclic mobility occurs, while for dense sand, liquefaction will never occur. Loose sand subjected to cyclic loading will liquefy under undrained condition but may be compacted to a denser state under drained condition.

In Zhang's model, the gradient of the *Critical State Line* (*C.S.L.*) is assumed to be constant and the flat ratio of the elliptical yield surface can be changed due to the anisotropy, as shown in Fig. A1(a). A new state variable ζ is introduced in the model, which is the stress-induced anisotropy and is assumed that the larger the ζ is, the larger the eccentric ratio of the ellipse will be. This feature enables the model to describe the cyclic mobility of sand during liquefaction, as shown in Fig. A1(b).

To verify the influence of the initial density on the behavior of sand, we herein numerically consider a set of sand samples with different densities, which is prepared from very loose sand. In preparing the set of sand samples with different densities, very loose sand is compacted by a small vibration load along the vertical direction with an amplitude level of 2.3 kPa and a small confining pressure of 10 kPa. After compaction, samples with different densities are isotropically consolidated to the prescribed confining pressure of 196 kPa. The samples are prepared with eight different densities at different levels of vibrating com-

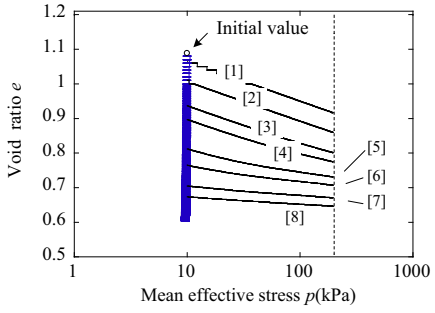

Fig. A2. Set of sand samples with different densities prepared from loose sand by vibration compaction and isotropic compression (Zhang et al., 2011).

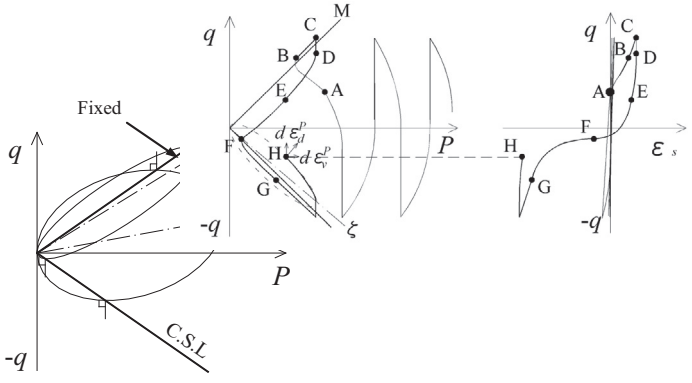

(a) Changes of yielding surface at different ζ (b) Stress-strain relations during cyclic mobility

Fig. A1. Changes of subloading yielding surface at different ζ and description of cyclic mobility.

paction, as shown in Fig. A2. The material parameters of Toyoura sand are listed in Table A1. The state variables of these sand samples after they are isotropically consolidated to a confining pressure of 196 kPa are listed in Table A2. With these material parameters and the initial values of the state variables for sands with different densities, various types of triaxial tests under drained/undrained conditions subjected to monotonic and cyclic loading are calculated systematically.

Table A1
Material parameters of Toyoura sand.

Compression index λ	0.050
Swelling index κ	0.0064
Critical state parameter M	1.3
Void ratio N (p = 98 kPa on $N.C.L.$)	1.0
Poisson's ratio v	0.30
Degradation parameter of overconsolidation state m	0.010
Degradation parameter of structure a	2.2
Evolution parameter of anisotropy b_r	1.5

From Fig. A3, it is seen that in undrained triaxial monotonic compression tests, loose sand exhibits peak strength at small levels of strain and then collapses and flows rapidly toward the origin of the stress space, showing typical strai n–hardening/softening and contractive behavior. For medium dense sand, the stiffness of the sand decreases abruptly at certain levels of strain where a typical transition from the contractive state to the dilative state occurs. Dense sand, however, only shows strain hardening. In the undrained tests, all of the sand samples finally move toward the *C.S.L.*, while in the drained tests, all of the sand samples approach the same point in the *e-p* space at the critical state, irrespective of the different initial densities at the beginning of shearing. The above-mentioned behavior of sand is very familiar to readers who specialize in soil mechanics, and thus, it is not necessary to give any comparison between the theoretical and the test results.

From Fig. A4, it is seen that the mechanical behavior of Toyoura sand subjected to cyclic loading under drained/

Table A2
State variables of Toyoura sand with different densities.

p = 196 kPa	[1]	[2]	[3]	[4]	[5]	[6]	[7]	[8]
e_0	0.916	0.860	0.801	0.775	0.731	0.707	0.671	0.646
R_0^*	0.104	0.114	0.125	0.133	0.149	0.160	0.172	0.179
OCR ($1/R_0$)	1.49	5.03	17.5	30.1	73.4	118.	255.	426.
ζ_0	1.44E−05	1.47E−05	1.97E−05	3.42E−05	5.95E−04	3.73E−03	2.18E−02	3.79E−02

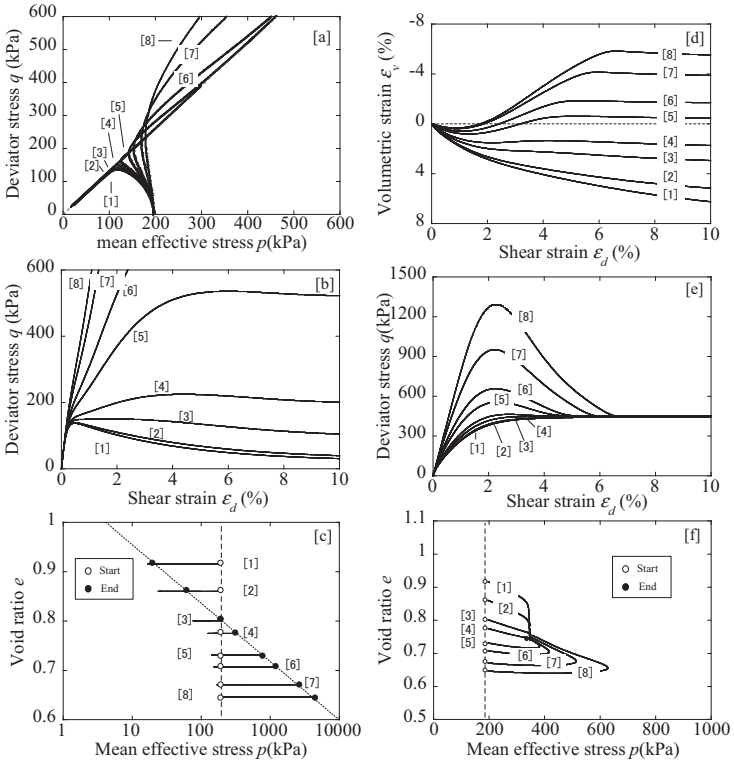

(a) Effective stress paths (b) Stress-strain relation (c) e-ln$p$ relation (d) Dilatancy (e) Stress-strain relation (f) e-p relation
(I) Undrained triaxial compression tests (II) Drained triaxial compression tests

Fig. A3. Simulation of Toyoura sand subjected to monotonic loading under different drained conditions in triaxial compression tests (Zhang et al., 2011).

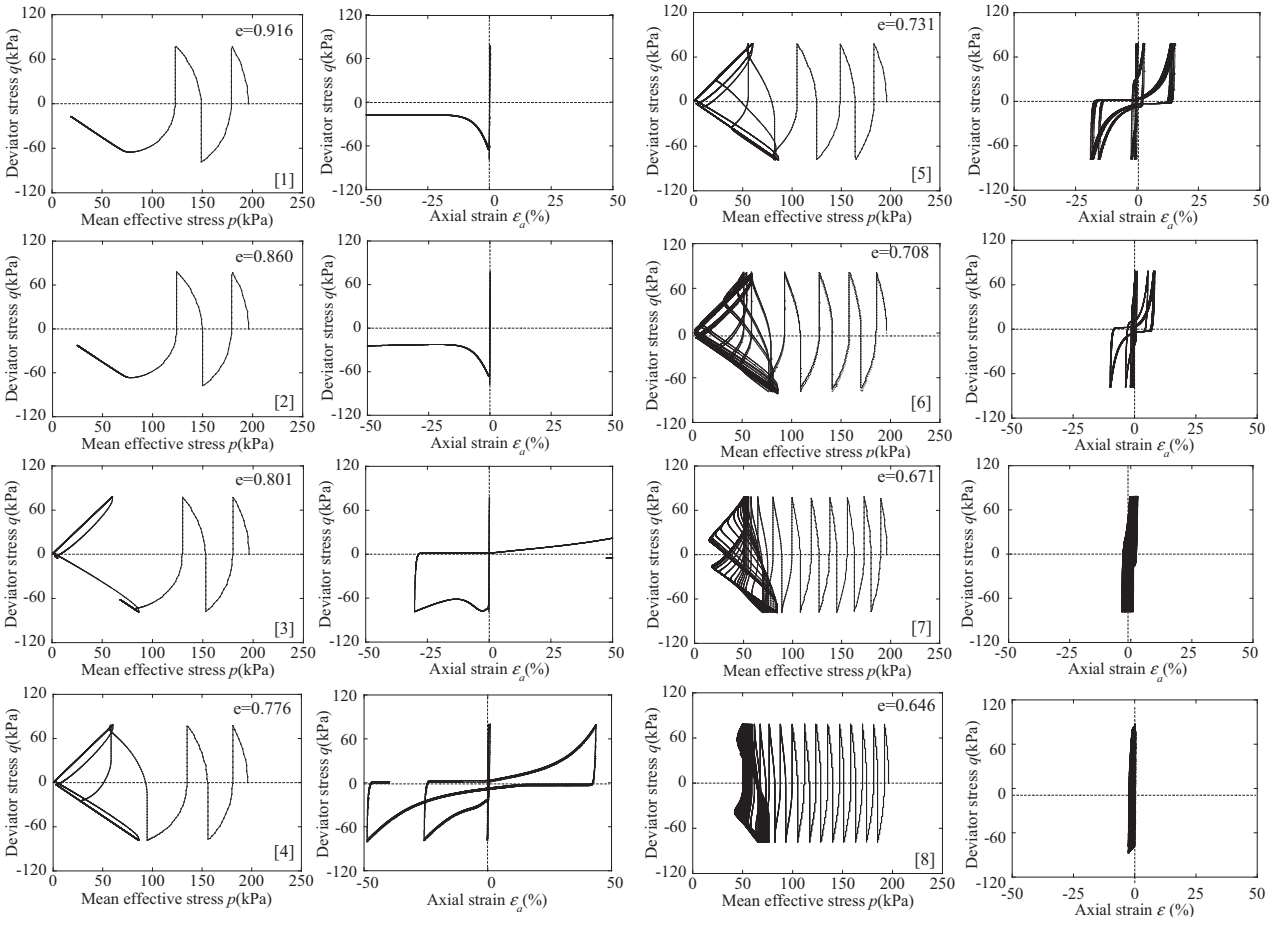

Fig. A4. Simulation of Toyoura sand subjected to cyclic loading under undrained conditions in triaxial compression tests (Zhang et al., 2011).

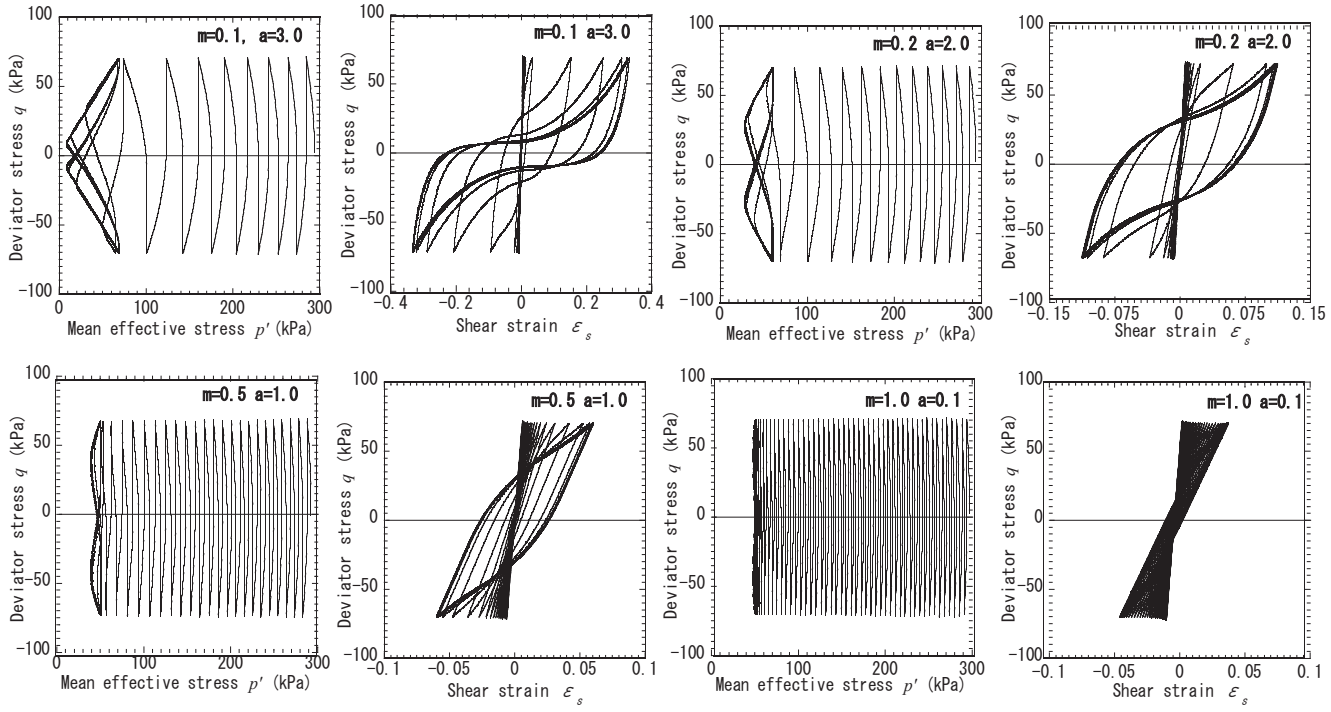

Fig. A5. Different types of behavior for sandy soils and clayey soils subjected to cyclic triaxial shear loading under undrained conditions (Zhang et al., 2007).

undrained conditions can be uniquely and properly described by the constitutive model no matter what the density is. It is confirmed theoretically that for loose sand, liquefaction happens without transitioning from the contractive state to the dilative state; for medium dense sand, cyclic mobility occurs, while for dense sand, liquefaction will not occur. It is not necessary to assign, in advance, which sand will liquefy or not. This is simply dependent on the state, namely, the overconsolidation ratio (density), stress-induced anisotropy and structure.

From Fig. A5, it is seen that the different types of behaviors for sandy soils and clayey soils subjected to cyclic loading under undrained conditions can be properly described by the constitutive model, by changing parameters a and m. The difference between clayey soils and sandy soils depends on two factors, namely, the rate of loss in overconsolidation and the rate of the collapse of structure during shearing (Asaoka et al., 2002). The rates of loss in overconsolidation and the collapse of structure are controlled by parameters a and m. For sandy soils, the rate of loss in overconsolidation is very slow (small m), while the rate of the collapse of structure is very fast (large a). On the contrary, for clayey soils, the rate of loss in overconsolidation is very fast (large m), while the rate of the collapse of structure is very slow (small a).

In summary, the mechanical behavior of Toyoura sand subjected to monotonic or cyclic loading under drained or undrained conditions can be uniquely and properly described by the constitutive model no matter what the density is. Moreover, the mechanical behavior of clayey soils can also be simulated by the model by changing parameters a and m.

References

American Society for Testing and Materials (ASTM) (2004). *Standard practices for obtaining undisturbed block (cubical and cylindrical) samples of soils*. West Conshohocken, PA: ASTM D7015-2004.

Asaoka, A., Nakano, M. and Noda. T. (1998). Super loading yield surface concept for the saturated structured soils. In*: Proc. of the fourth European conference on numerical methods in geotechnical engineering-NUMGE98* (pp. 232–242).

Asaoka, A., Noda, T., Yamada, E., Kaneda, K., & Nakano, M. (2002). An elasto-plastic description of two distinct volume change mechanisms of soils. *Soils and Foundations, 42*(5), 47–57.

Bao, X. H., Ye, G. L., Ye, B., Sago, Y., & Zhang, F. (2014). Seismic performance of SSPQ retaining wall—Centrifuge model tests and numerical evaluation. *Soil Dynamics and Earthquake Engineering, 61–62*, 63–82.

Bao, Y. F., Ye, G. L., Ye, B., & Zhang, F. (2012). Seismic evaluation of soil foundation superstructure system considering geometry and material nonlinearities of both soils and structures. *Soils and Foundations, 52*(2), 257–278.

Becker, D. E., Crooks, J. H. A., Been, K., & Jefferies, M. G. (1987). Work as a criterion for determining in situ and yield stresses in clays. *Canadian Geotechnical Journal, 24*(4), 549–564.

Callisto, L., & Rampello, S. (2004). An interpretation of structural degradation for three natural clays. *Canadian Geotechnical Journal, 41*(3), 392–407.

Chai, J. C., Shen, S. L., Zhu, H. H., & Zhang, X. L. (2004). Land subsidence due to groundwater drawdown in Shanghai. *Géotechnique, 54*(2), 143–147.

Chen, J. J., Zhang, L., Zhang, J. F., Zhu, Y. F., & Wang, J. H. (2013). Field tests, modification and application of deep soil mixing (DSM) method in soft clay. *Journal of Geotechnical and Geoenvironmental Engineering, ASCE, 139*(1), 24–34.

Dafalias, Y. F., & Popov, E. P. (1975). A model of nonlinearly hardening materials for complex loading. *Acta Mechanica, 21*(3), 173–192.

De'an, Sun., Bo, Chen., & Changfu, Wei. (2014). Effect of fabric on mechanical behavior of marine clays. *Marine Georesources & Geotechnology, 32*(1), 1–17. http://dx.doi.org/10.1080/1064119X.2012.710714.

Gao D.Z., Wei D.D. and Hu Z.X. (1986). Geotechnical properties of Shanghai soils and engineering applications. In: R.C. Chaney, Fang, H.Y. (Ed*.), ASTM special technical publication 923 marine geotechnology and nearshore-offshore structures* (pp. 161–177).

Hashiguchi, K., & Ueno, M. (1977). Elastoplastic constitutive laws of granular material, Constitutive Equations of Soils. In S. Murayama, & A. N. Schofield (Eds.), *Proc. 9th ICSMFE, Spec. Ses. 9* (pp. 73–82). Tokyo: JSSMFE.

Hou, Y. M., Wang, J. H., & Zhang, L. L. (2009). Finite-element modeling of a complex deep excavation in Shanghai. *Acta Geotechnica, 4*(1), 7–16.

Huang, Y., Ye, W. M., & Chen, Z. C. (2009). Seismic response analysis of the deep saturated soil deposits in Shanghai. *Environmental Geology, 56*(6), 1163–1169.

Jin, Y., Ye, B., & Zhang, F. (2010). Numerical simulation of sand subjected to cyclic load under undrained conventional triaxial test. *Soils and Foundations, 50*(2), 177–194.

Kimoto, S., & Oka, F. (2005). An elasto-viscoplastic model for clay considering destructuralization and consolidation analysis of unstable behavior. *Soils and Foundations, 45*(2), 29–42.

Li, Q., Ng, C. W. W., & Liu, G. B. (2012). Determination of small-strain stiffness of Shanghai clay on prismatic soil specimen. *Canadian Geotechnical Journal, 49*(8), 986–993.

Liu, M. D., & Carter, J. P. (2002). A structured Cam Clay model. *Canadian Geotechnical Journal, 39*(6), 1313–1332.

Liu, G. B., Ng, C. W. W., & Wang, Z. W. (2005). Characteristics of wall deflections and ground surface settlements in Shanghai. *Journal of Geotechnical and Geoenvironmental Engineering, 131*(8), 1004–1013.

Mita, K. A., Dasari, G. R., & Lo, K. W. (2004). Performance of a three-dimensional Hvorslev-Modified Cam Clay model for overconsolidated clay. *International Journal of Geomechanics, 4*(4), 296–303.

Muir Wood, D., Belkheir, K., & Liu, D. F. (1994). Strain softening and state parameter for sand modelling. *Géotechnique, 44*(2), 335–339.

Nakai, T., & Hinokio, M. (2004). A simple elastoplastic model for normally and overconsolidated soils with unified material parameters. *Soils and Foundation, 44*(2), 53–70.

Peng, F., Wang, H., Tan, Y., Xu, Z., & Li, Y. (2011). Field measurements and finite-element method simulation of a tunnel shaft constructed by Pneumatic Caisson Method in Shanghai soft ground. *Journal of Geotechnical and Geoenvironmental Engineering, ASCE, 137*(5), 516–524.

Rouainia, M., & Muir Wood, D. (2000). A kinematic hardening model for natural clays with loss of structure. *Géotechnique, 50*(2), 153–164.

Sekiguchi H, Ohta K. (1977). Induced anisotropy and time dependence in clays. In: *Constitutive equations for soils. Proceedings of 9th ICSMFE (Specialty Session 9)*, Tokyo, Japan (pp. 229–238).

Shen, S. L., Horpibulsuk, S., Liao, S. M., & Peng, F. L. (2009). Analysis of the behavior of DOT tunnel lining caused by rolling correction operation. *Tunnelling and Underground Space Technology, 24*, 84–90.

Shen, S. L., Wu, H.-N., Cui, Y.-J., & Yin, Z. Y. (2014). Long-term settlement behaviour of metro tunnels in the soft deposits of Shanghai. *Tunnelling and Underground Space Technology, 40*, 309–323.

Shen, S. L., & Xu, Y. S. (2011). Numerical evaluation of land subsidence induced by groundwater pumping in Shanghai. *Canadian Geotechnical Journal, 48*(9), 1378–1392.

Tan, Y., & Wei, B. (2012). Observed behavior of a long and deep excavation constructed by cut-and-cover technique in Shanghai soft clay. *Journal of Geotechnical and Geoenvironmental Engineering, ASCE, 138*(1), 69–88.

Wang, J. H., Xu, Z. H., & Wang, W. D. (2010). Wall and ground movements due to deep excavations in Shanghai soft soils. *Journal of Geotechnical and Geoenvironmental Engineering, ASCE, 136*(7), 985–994.

Wei, D. D., & Hu, Z. X. (1980). Experimental study on the preconsolidation pressure and compressibility parameters of Shanghai Subsoil. *Chinese Journal of Geotechnical Engineering, 2*(4), 13–22 (in Chinese with English abstract).

Whittle, A. J., & Kavvadas, M. J. (1994). Formulation of MIT-E3 constitutive model for overconsolidated clays. *ASCE Journal of Geotechnical Engineering, 120*(1), 173–198.

Wu, C. J., Ye, G. L., Zhang, L. L., Bishop, D., & Wang, J. H. (2014). Depositional environment and geotechnical properties of Shanghai clay: A comparison with Ariake and Bangkok clays. *Bulletin of Engineering Geology and the Environment*. http://dx.doi.org/10.1007/s10064-014-0670-0.

Xia, Z. F., Ye, G. L., Wang, J. H., Ye, B., & Zhang, F. (2010). Fully coupled numerical analysis of repeated shake-consolidation process of earth embankment on liquefiable foundation. *Soil Dynamics and Earthquake Engineering, 30*(11), 1309–1318.

Xu, Y. S., Shen, S. L., & Du, Y. J. (2009). Geological and hydrogeological environment in Shanghai with geohazards to construction and maintenance of infrastructures. *Engineering Geology, 109*(3–4), 241–254.

Ye, B., Muramatsu, D., Ye, G. L., & Zhang, F. (2011). Numerical assessment of vibration damping effect of soilbags. *Geosynthetics International, 18*(4), 159–168.

Ye, B., Ye, G. L., & Zhang, F. (2012). Numerical modeling of changes in anisotropy during liquefaction using a generalized constitutive model. *Computers and Geotechnics, 42*, 62–72.

Ye, B., Ye, G. L., Zhang, F., & Yashima, A. (2007). Experiment and numerical simulation of repeated liquefaction-consolidation of sand. *Soils and Foundations, 47*(3), 547–558.

Yin, Z.-Y., Karstunen, M., Chang, C. S., Koskinen, M., & Lojander, M. (2011). Modeling time-dependent behavior of soft sensitive Clay. *Journal of Geotechnical and Geoenvironmental Engineering, ASCE, 137*(11), 1103–1113.

Zhang, F., Ye, B., Noda, T., Nakano, M., & Nakai, K. (2007). Explanation of cyclic mobility of soils: Approach by stress-induced anisotropy. *Soils and Foundations, 47*(4), 635–648.

Zhang, F., Ye, B., & Ye, G. L. (2011). Unified description of sand behavior. *Frontiers of Architecture and Civil Engineering, 5*(2), 121–150.